Chapter 3

Label free spectroscopic determination of formation of and molecular packing in cyclohexane based hydrogelator fibres

Abstract

Gelation of water with small molecules (hydrogelators) sees continued interest ranging from biological and medical applications to soft robotics. The design of hydrogelators is largely hit and miss and largely focuses on the serendipitous balancing of the multiple intra- and inter-molecular interactions. Achieving specific properties by design however is still well beyond the state of the art. Rational design of gelators requires understanding both the interactions involved at multiple hierarchical levels and the actual dynamic processes involved. Typically the low concentrations of gelator molecules necessitates the use of molecular probes, often based on fluorescence, however these probes can disrupt the processes being studied. Here we report the elucidation of the mechanism by which C_3-symmetric hydrogels form using a combination of dark field microscopy, cryo-TEM, small angle X-ray scattering, polarized Raman and single crystal X-ray structures the gelation can be followed from microscopic to macroscopic growth. The aggregate data allows for validation of a postulated mechanism and model which will form the basis of a more rational approach to gelator design.

Introduction

Hydrogels are ubiquitous and are the basis for materials with applications as diverse as soft robotic materials, sensing and smart drug delivery, and of course life.[1–5] Synthetic hydrogels can enable building in of response to external stimuli such as pH change, light, foodstuffs and shock, to name but a few.[6–9] Hydrogels based on low molecular weight compounds (hydrogelators) are especially attractive since they are intrinsically well-defined in composition, toxicity profile and enable tuning of properties through systematic structural variations. The design of potential hydrogelators typically focuses on anisotropic supramolecular stacking directed by H-bonding (e.g., amide or urea groups), Van der Waals (stacking of aliphatic chains) and π-π interactions.[10–14] These anisotropic intermolecular interactions result in the growth of fibre like structures and from which an interlocking three dimensional matrix of fibres can form that shuts down convective mass transport.

Prediction of the behaviour of compounds that have the potential to form hydrogels through such anisotropic interactions is still at best intuitive. A rational approach necessitates understanding why some compounds gelate water while analogues, with only minor structural differences, do not form hydrogels.[15–17] Indeed, models for the arrangement of molecules in gel fibres available are essentially all based on analogy to the structure of the same or similar compounds as single crystals (determined by X-ray diffraction) rather than direct structural analysis of the gel fibres. For example, models for the packing in BTA (benzene triamide), cyclohexane triamide, and Fmoc based supramolecular polymers and gels are based on crystal structures of the compounds **BTA-Me**, **CH-Tyr** (Figure 1) and **Fmoc-F**, respectively.[15,18,19] It is notable that none of these model compounds have been reported to form gels and, as we will show here, such analogies between crystal structures and molecular arrangement in gel fibres can prove false.

The low concentration of hydrogelating compounds in gels (typically < 1 % by mass) presents a central challenge to direct efforts. Nevertheless assembled supramolecular structures can be probed by circular dichroism spectroscopy, wide field, super resolution, and fluorescence microscopy, and DFT methods.[20] For emission based methods the reporter molecules (e.g., fluorophores) can potentially disrupt the delicate gelation and self-assembly process.[21] Furthermore, although the intermolecular alignment and interactions in gel fibres is modelled largely on by analogy with interactions found in single crystal X-ray structures of analogues, to the best of our knowledge a direct correlation between the structures adopted in single crystals and gel fibres has not been made. Furthermore, the mechanism by which gel fibres form to gelate the solvent is largely perceived to be kinetically driven, i.e. fibres form depleting the solution of non-aggregated monomers more rapidly than single crystal growth can take place. This model may not hold in all cases. Hence, evidence based models for the driving forces behind gelation and the intramolecular interactions responsible are essential

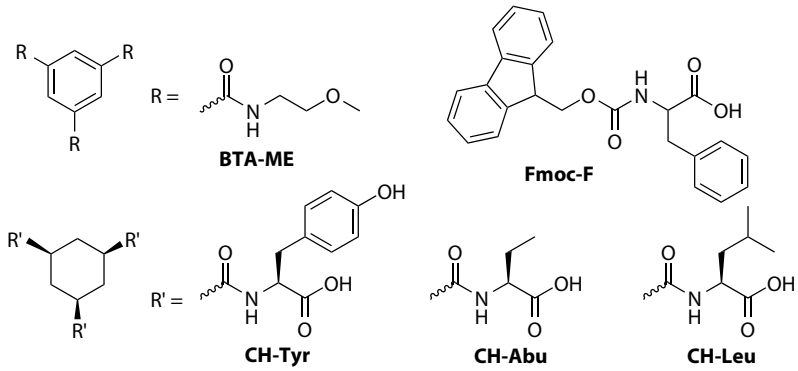

Figure 1. *Structures of compounds described in the text.*

to prediction and rational design of hydrogelators.

The hydrogelators used here are based on a cyclohexane core were first reported in 2002.[22] Subsequent studies focused on the effect of variation in molecular structure on gelation properties.[19,23–26] This class of gelators has since shown utility in dissipative systems in which formation and destruction proceed concomitantly to create a dynamic gel matrix.[27,28] Efforts at real time studies of gel formation by fluorescence microscopy to date have necessitated the use of additives and co-solvents that can be expected to perturb the system also and indeed, as shown in the present study, co-solvents have a significant effect on the gel formation times.[29]

The key structural motifs in these gelators are the cyclohexyl-triamide core and interactions between the amino acid based side groups, suggesting a stacking arrangement where the acid groups are in proximity and anionic repulsion is mitigated by protonation and/or cation binding.[19] Indeed gel fibre formation occurs only under mildly acidic conditions. The single crystal X-ray structure of **CH-Tyr**, which was reported earlier not to engage in solvent gelation, indicates that linear stacking of the cyclohexane units forms the core structure with intermolecular hydrogen bonding of the amides. Recently we reported that D_2O and salts have a substantial impact on gel properties through perturbing intermolecular forces,[17] which highlight the complexity of the interactions that lead to anisotropic growth of fibres. The central challenge faced in the design of gelators is to establish the packing of the gelator molecules in the gel fibres, however, to date models have drawn on analogy and best guess rather than direct evidence. This dearth of information is unsurprising considering that the gelators under investigation here, **CH-Abu** and **CH-Leu**, show critical gelation concentrations (CGC) of 7.5 and 6 mg/mL respectively, and do not show UV-Vis absorbance, CD signals, nor are they detectable by FTIR spectroscopy in the gelled state.

Here, we show through a combination of label free techniques that the correspondence between crystal structures and molecular packing in the gel fibres is coincidental but that direct spectroscopic analysis using polarisation dependent Raman microspectroscopy can confirm the molecular packing state. Through a combination of techniques we probe the time dependence of hydrogelation by **CH-Abu** and **CH-Leu**, from the micron scale using darkfield microscopy to the nm range using cryo-TEM and SAXS, which together allow us to establish a model for gel formation including possible off paths, e.g. crystallization, amorphous precipitation, etc.

Results

Gelation of this class of compounds can be achieved by first dissolving the monomers in water, either by heating or at a high pH (Figure 2). Then a trigger is needed for the gelation to occur, e.g. cooling or a pH drop upon adding acid (Figure 2, lower pathway). In this path, first small fibres and amorphous precipitation form. The small fibres grow over time creating a gel fibre network and thereafter the fibres enlarge, either by incorperating more monomer or by entanglement. However, when subjected to this trigger the gelator can also precipitate (Figure 2 top right) or form crystals (Figure 2, top left) and hence gel formation requires a balance between the extent of precipitation/crystallization and gel fibre formation. In the case of the gels discussed here stable gels form readily by either pathway but with small amount of amorphous precipitation.

Label free analysis of gelators is crucial because adding even small amounts of other components can affect drastically gelation properties and formation times.[21] We have shown earlier that adding salts and D_2O leads to changes in melting points and CGCs for **CH-Abu** and **CH-Leu**.[17] DMSO, used commonly to solubilise hydrophobic probes, does not disrupt gelation but delays the onset of opacity (Figure 3) manifested in a non-linear increase in light scattering after a delay. The delay is dependent on the vol% DMSO present (Figure 3). The influence of DMSO on gelation kinetics precludes the use of common additives that need prior dissolution in co-solvents.

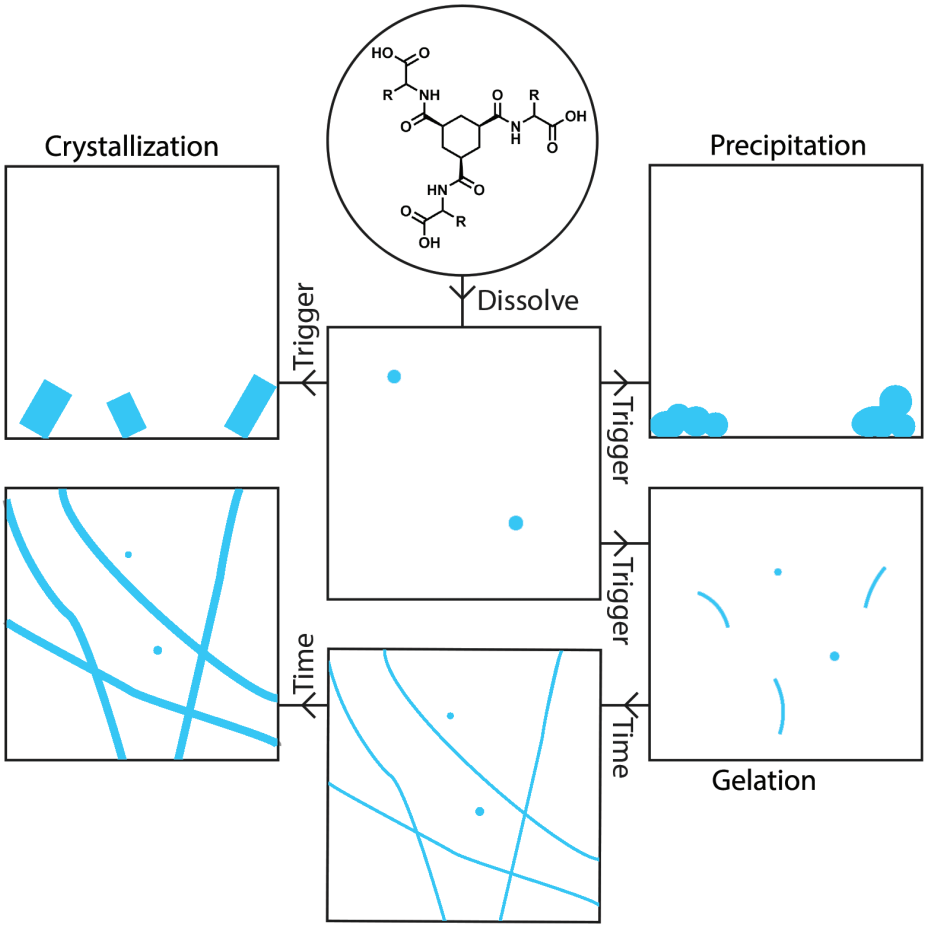

Figure 2. *Proposed model for all possibilities during dissolving and gel triggers.*

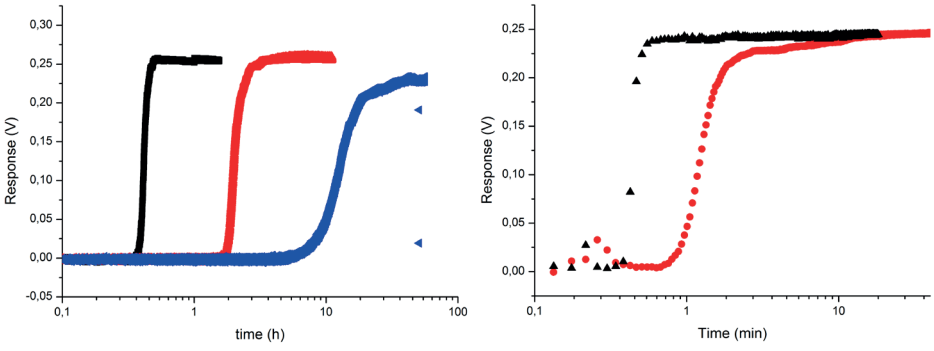

Figure 3. *Scattering profile of a)* ***CH-Abu*** *with 0v/v% DMSO (black), 5 v/v% DMSO (red), and 10 v/v% (blue) b)* ***CH-Leu*** *with 0v/v% DMSO (black) and 5 v/v% DMSO (red).*

Although in the gel state the monomers contained within the fibres are not free to diffuse and hence their signals are absent in the ^{1}H-NMR spectrum, the unbound monomer is observed readily. Gels were prepared by addition of $DCl_{(aq)}$ to **CH-Abu** (8 mg/mL) or **CH-Leu** (7.5 mg/mL) in NaOD in D_2O with 0.05 vol. % DMSO as an internal reference. Addition of D_2O in place of $DCl_{(aq)}$ provided a fully dissolved reference sample. In all samples, the expected ^{1}H NMR spectra of the fully dissolved monomers were observed, however, for both gelators the signal intensity was only 10% that of the reference samples. These data are consistent with 90% of the gelator molecules immobilized within the gel fibres. DOSY ^{1}H NMR spectroscopy confirms that the diffusion rate constant of the monomers is the same in gels as in the reference samples ca. 5×10^{-6} cm^2 s^{-1}. Furthermore, these data indicate that dissolved monomers present in the gel state, i.e. those not incorporated in the gel fibres, exchange between monomers in the gel fibres slowly (i.e. > 5 ms), which is consistent with the linear growth of the fibres observed macroscopically (vide infra).

Dark field microscopy

The difference in refractive index between the gel fibres and solvent enable real time observation of gel formation by dark field microscopy. Addition of acid to a basic solution of monomers results in immediate formation of particles as bright spots (ø < 200 nm, supporting video 1 and 2, Figure 4 A/D). These particles show translational motion due to convection (video 3 and 4). After a certain time they slow and eventually their translational movement appears to be confined to within a relatively small region, typically ca. 4 μm box (supporting video 5 and 6), indicating that translation motion (convection) has ceased and the solution has become a gel. However, the fibres are not yet visible by microscopy. Only after the particles' translational freedom has been restricted do fibres appear as fast growing structures; the bright lines, through the field of view (supporting video 7 and 8, Figure 4 B, C, E & F). The growth of the fibres observed by dark field microscopy is anisotropic (linear, 7.4 μm/s) with long fibrous structures formed with no apparent branching for **CH-Abu**. In contrast, for **CH-Leu** a highly branched network is formed (2.7 μm/s) with fibres extending outwards from a core bundle. This difference in structure may be related to the increase in steric hindrance from the leucine side groups. However, it is of note that in all of the experiments fibre growth was not initiated (nucleated) at a particle.

The appearance of the fibre like structures only after the translational motion of the particles becomes restricted indicates strongly that initially a network of thinner fibres (i.e. too narrow to provide significant scattering of light) is formed. It is these thinner fibres that are, at least initially, responsible for gelation of the solution, with the thicker (observable) fibres forming later either reinforcing the gel structure or replacing the initially formed scaffold.

Cryo-TEM of CH-Leu and CH-Abu at time interval

The formation of thin fibres in the initial stages of gelation was confirmed by Cryo-TEM studies. Samples of solutions of **CH-Leu** were frozen in liquid ethane over a range of times following addition of acid (Figure 5). Samples frozen immediately after acidification (< 10 s, Figure 5 A/B) presented short fibres with an average thickness of around 21 (+/- 5 nm). The thickness of the fibres increased with time delay before freezing to 28.5 and 32 nm (+/- 4 nm), at 20 and 120 s (Figure 5 C-F), respectively. Gels allowed to mature overnight presented fibres with a thickness of 135 nm (+/- 29, Figure 5 G-H). It is notable that the sample frozen within 10 s presented amorphous particles with a diameter of ca. 304 (+/- 50) nm that were absent entirely in samples at a later stage. These spherical objects correspond to those observed by dark field microscopy.

Diffraction patterns measured from the fibres observed in the 24 h matured gel of **CH-Leu** by cryo-TEM show the two ring diffractions expected from amorphous water,[30] which provide a reference for the packing distance of a repeating unit in the fibres (Figure 5 I). The repeat distance is 4.9 Å, which corresponds to the inter ring distance observed in the single crystal structure of **CH-Tyr** of

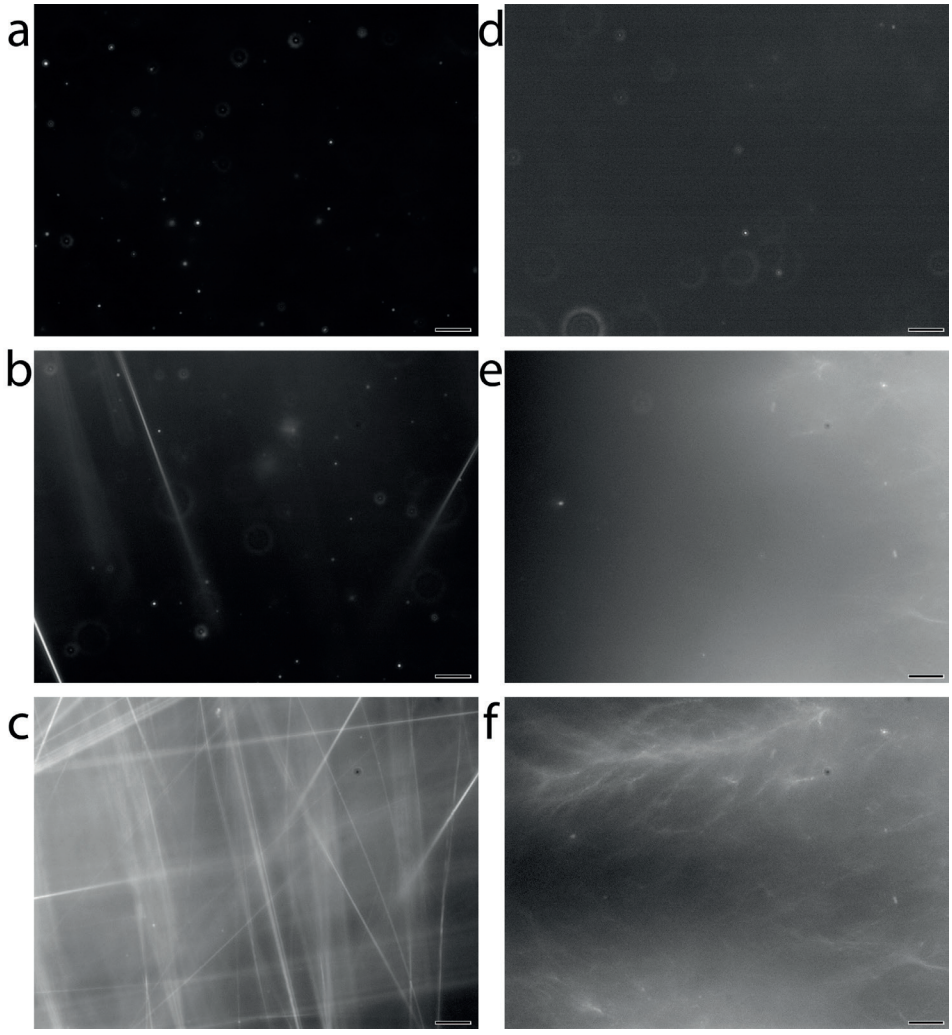

Figure 4. *Dark field microscope images of* ***CH-Abu*** *and* ***CH-Leu*** *a)* ***CH-Abu*** *just after mixing (44 s) b)* ***CH-Abu*** *at the start of fibre formation (264 s) c)* ***CH-Abu*** *at the point were no more movement is observed (352 s). d) CH-L.eu just after mixing (49 s). e)* ***CH-Leu*** *at the start of fibre formation (150 s). f)* ***CH-Leu*** *at the point were no more movement is observed (180 s). Scale bar is 10 µm.*

4.9 Å and not the inter ring distance of 6.5 Å for the **CH-Abu** single crystal structure (vide infra). These data support that the packing of **CH-Leu** in the fibres is similar to the packing of **CH-Tyr** in the crystal.[19]

Cryo-TEM images of **CH-Abu** present star burst patterns of fibres when frozen within 2 min while samples frozen at 10 min show only dense organic matter consistent with radiation damage. Radiation damage and interference from the blotting and freezing process due to the length of time taken for **CH-Abu** to form a gel on the TEM-grid reduces the quality of gel fibres formed and cause precipitation. These effects precluded time dependent analysis. Cryo-TEM analysis of matured (overnight) **CH-Abu** gels show 147 nm (+/- 50) diameter fibres.

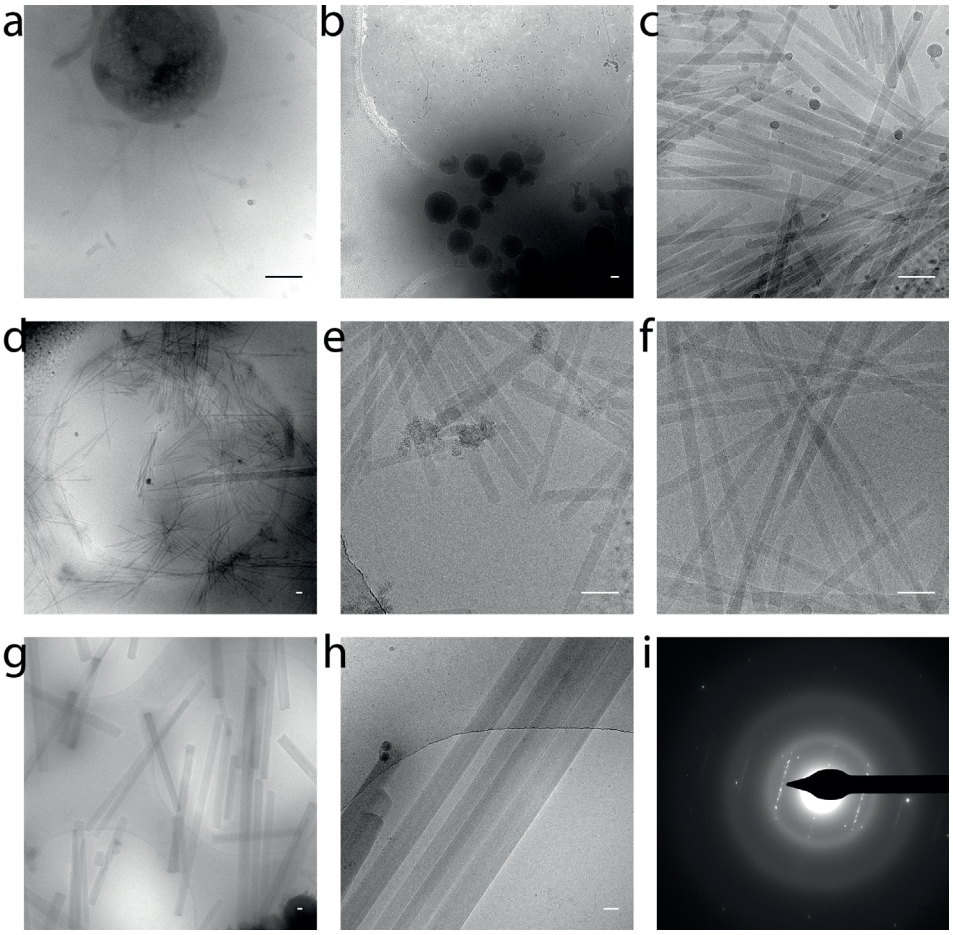

Figure 5. *Cryo-TEM images of* ***CH-Leu*** *after a) 10 s b) 10 s c) 20 s d) 20 s e) 120 s f) 120s g) 24 h h) 24 h i) electron diffraction of* ***CH-Leu*** *after 25 h, Scale bar for all cryo-TEM images 100 nm.*

The fibres present at any stage are of uniform thickness over their whole width as well as length, consistent with flat ribbon structures rather than cylinders. Synchrotron small-angle X-ray scattering (SAXS) was employed to follow gelation by **CH-Leu** in real time.

Time profile of SAXS of CH-Leu

SAXS profiles over time (Figure 6 A) show that a signal for q values below 0.2 nm^{-1} at 30 s. The intensity shows a power law decay with a mild inflexion at the low angles in the log(I) *vs* log(q) plot. This is indicative of the presence of nanostructure in the probed range. Analysis of the scattering curve with a Debye-Bueche model for nanostructures with spherical symmetry provides a characteristic length scale for the scattering objects of about 38 nm (Figure 6 B). Interestingly, within only 5 s a drastic intensity increase together with a pronounced change of curve shape occur. The SAXS curve at t = 35 s shows a different slope in the log-log plot at the lowest q values, together with one distinct oscillation in the intermediate explored q range. This large change is due to the formation of elongated objects. With time, the intensity at low q values increases steadily, while the intensity oscillation moves towards small q values and becomes less pronounced. The calculated slope at t = 35 s is -1.9.

Usually, a slope of -1 is expected for rod-like objects with circular cross-section while anisotropic flat objects show a -2 slope in the log-log plot. The intermediate slope suggests the presence of elongated objects (in agreement with TEM measurements discussed above) with non-circular cross-section (elliptical or rectangular). The SAXS intensity for both 35 s and 695 s was modelled to extract the size of the scattering objects. Figure 6 C/D show the best fit curves obtained using analytical models for elongated objects with circular and elliptical cross-section. The model using elliptical cross-section provides consistently better agreement with respect to the experimental data, especially in the low q region. The short and long semi axis of the aggregate cross-section are calculated to be about 15 and 24 nm at 35 s, respectively. Over time, the aggregates grow reaching a dimension of about 18 x 70 nm after 695 s.

In both cases, the length of the elongated aggregates is larger than the maximum distance observed by SAXS as visible in the DFM and cryo-TEM (>200 nm). These values suggest that the molecules aggregate in a 3D fashion but exhibit preferential 1D aggregation, with higher aggregation in the direction of the intermolecular hydrogen bonds of the amide bonds. The SAXS fitting also shows how the elongated aggregates have very uniform cross-section at the beginning (t = 35 s) and more heterogeneous cross-sectional dimensions at the end of the aggregation process. The results of the SAXS modelling are in agreement with the shape and dimensions observed by TEM and can be further validated by Guinier analysis of the cross-section.[31,32] The cross-sectional radius for the ag-

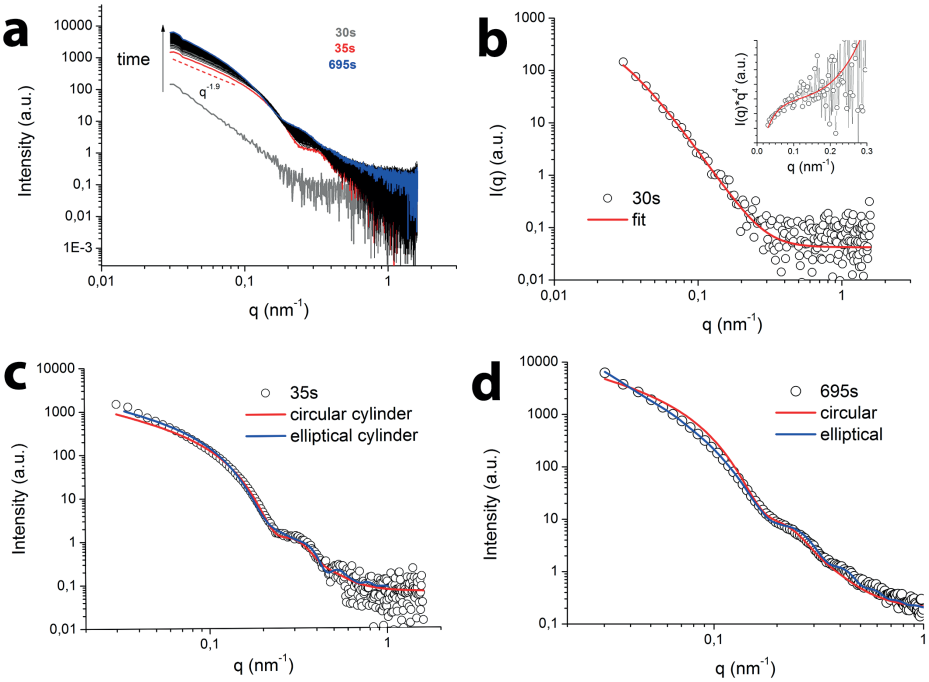

Figure 6. *a) SAXS intensity evolution as a function of time. Three critical time values are highlighted in grey (30s), red (35s) and blue (695s). b) SAXS profile at 30s together with the best fit using a Debye-Bueche model plus a constant background. The inset shows the SAXS intensity and the fit multiplied by the q4 to highlight the shape of the scattering curve at the lowest q values. c) SAXS profile at 695s together with the best fit using rod-like shape objects with circular cross-section (red curve) and elliptical cross-section (blue curve). d) SAXS profile at 35s together with the best fit using rod-like shape objects with circular cross-section (red curve) and elliptical cross-section (blue curve).*

gregates at t = 35 s is R_c = 18.5 nm as calculated from the slope of the data in the Ln[I(q)q^2] *vs* q^2 plot in the range $qR_c < 1$ (see Figure 6), in close agreement to the value found by best fit using the elliptical cross-section (R_c = 19 nm).

Dark field microscopy, cryo-TEM and SAXS support a model in which initially small fibres appear followed by growth of larger (thicker) fibres. The molecular packing with these structures is key to the success of these gelators and insight into possible packing arrangements can be gleaned from single crystal X-ray analysis. We obtained single crystals of **CH-Abu** suitable for diffraction from aqueous solutions below the critical gelation concentration (CGC), which, considering that it forms gels under these conditions, should provide insight into intermolecular packing within the gel fibres. However, connecting the X-ray structure with packing in gel fibers requires comparison of spectral and especially anisotropic character of the spectral properties of the crystal and fibers. Polarization dependent Raman spectroscopy proved invaluable in determining the conformation and orientation of the building blocks within the crystal and dried gel fibres.

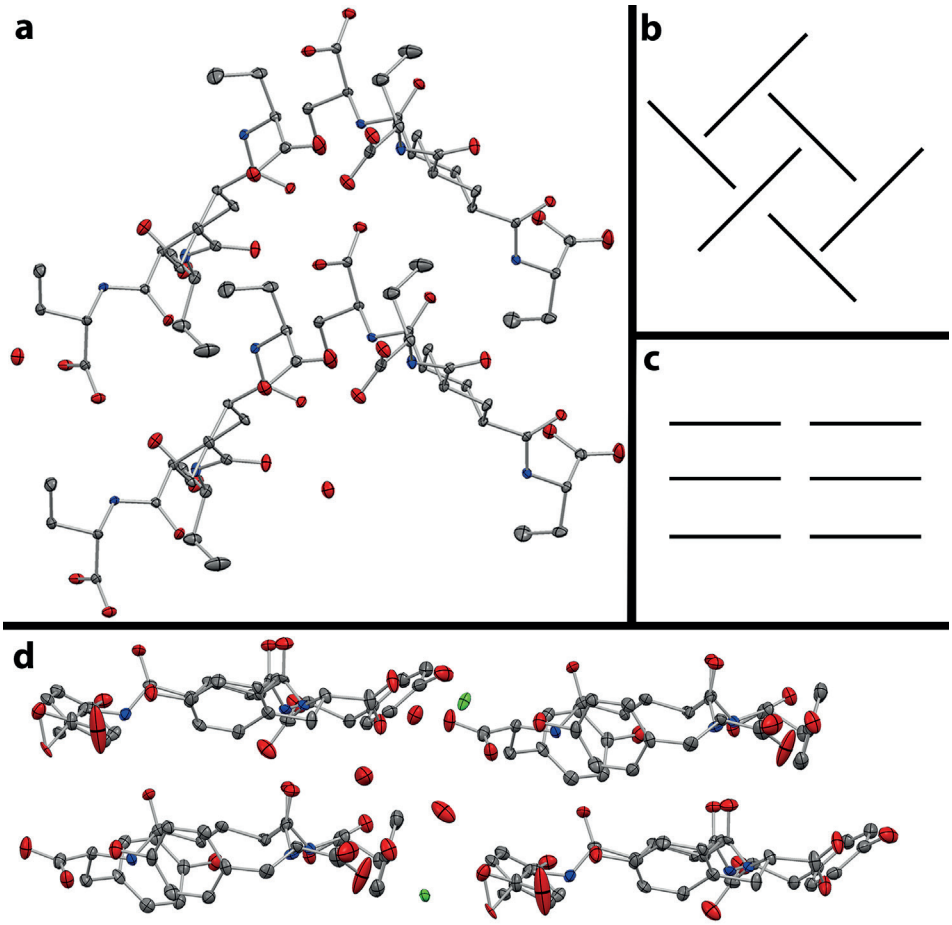

Figure 7. *a) Crystal packing of four monomers of* ***CH-Abu****. b) Schematic crystal packing in a herringbone fashion of* ***CH-Abu****. c) Schematic crystal packing of stacked discs of* ***CH-Tyr****. d) Crystal packing of four monomers of* ***CH-Tyr****.*

Crystal structure and its relation to gel fibres for CH-Abu

The single crystal X-ray structure for **CH-Abu** shows packing in a herringbone fashion in contrast to the two crystal structures reported earlier for structurally related cyclohexane core and benzene core compounds (Figure 7).[19,33] The structures reported previously all show stacking of the core (cyclohexane or benzene) in a linear manner with three equivalent intermolecular hydrogen bonds to the same neighbour in the stack. In the present case, **CH-Abu**, the hydrogen bonding and stacking arrangement is different. The unit cell contains two monomer units and only one amide in each of the monomers engages in hydrogen bonding to the other monomer in the unit cell (Figure 7). The other hydrogen bonding interactions are either to one of the carboxyl groups or to water of crystallization. The distance between the rings is 6.573 Å and is further that for the structures of analogues reported earlier, e.g. 4.972 Å in the structure of **CH-Tyr**.[19]

Raman of CH-Tyr and CH-Abu crystals and CH-Abu fibres

Raman spectra were recorded using polarized laser excitation to determine the orientation of bonds within the fibre through the dependence of Raman scattering intensity on polarization direction with respect to the crystal or fibre axes of **CH-Abu**. Three N-H stretching bands (~3200 cm^{-1}) and three amide I (~1600 cm^{-1}) bands are observed in the spectra of the single crystal while only one N-H stretch and one amide I band in the gel (Figure 8 A/B). These data show that the molecular packing in the crystal is different from that in the fibre. The reduced number of bands is consistent with an increase in symmetry in the case of the gel fibres. The gel fibres show a response to the polarization with a period of 180°. Both amine and amide peaks show polarization dependence on the intensity of the bands indicating that they are aligned in the same direction. The maximum of the amide bands is not coincident with fibre long axis but instead at

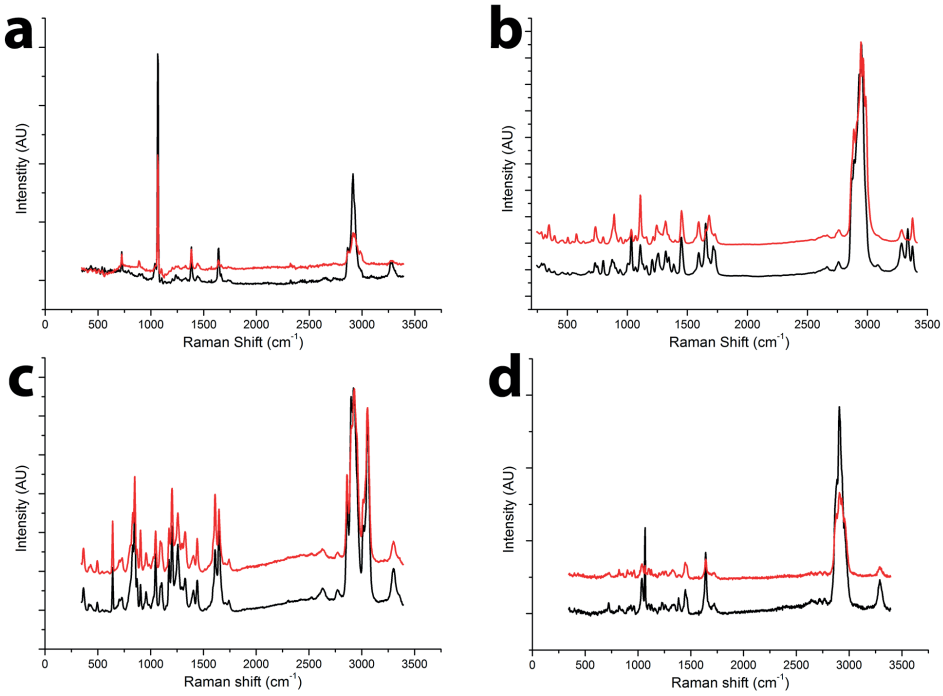

Figure 8. *Polarized Raman Spectra of a)* ***CH-Abu*** *fibres b)* ***CH-Abu*** *crystal c)* ***CH-Tyr*** *crystal d)* ***CH-Leu*** *fibre, black maximum intensity N-H stretch, red minimum intensity N-H stretch.*

20° indicating that the amides are not fully aligned in the direction of the long axis of the fibre.

The polarization dependence of the Raman spectra of the single crystal shows three amide N-H bands consistent with the three distinct amides present in the unit cell. The edge of the crystal corresponds to the b axis in the crystal and was taken as the reference (i.e. 0°). Most of the amide I and N-H stretch bands show highest intensity when excited along this axis, which corresponds to their orientation in the crystal, while the band at 1687 cm^{-1}, corresponding to an amide I stretch is oriented differently.

For **CH-Leu** gel fibres we observe only a single N-H stretch and C=O stretch, indicating similar packing to that in the **CH-Abu** fibres (Figure 8 D). the packing model in the present case is based on crystal structures for two analogues of the cyclohexane based gelators.[19,33] Our crystals prepared from **CH-Tyr**, using the procedure reported earlier,[19] have the same unit cell and packing. The polarized Raman spectra of these crystals show a single N-H stretching bands and one C=O Amide I band, which indicate that the fibres of **CH-Abu** and **CH-Leu** stack in a similar manner to that in the **CH-Tyr** crystal than in the single crystal obtained for **CH-Abu** (Figure 8 C).

Discussion

The cumulative data described earlier[17,19] and here provides for a detailed model of both the molecular structures that form gel fibres and the mechanism and factors that drive their formation. Acidification of basic solutions results in a sudden order of magnitude decrease in solubility due to protonation of the gelator molecules and the formation of amorphous aggregates (< 200 nm). The formation of a network of fibres is manifest in the loss of linear translational (convection) motion of the particles. Initially the network is comprised of thin fibres, which, although not observable by optical microscopy, are observed by SAXS and in cryo-TEM micrographs. Furthermore, the cryo-TEM micrographs and SAXS data are consistent with formation of tape-like structures rather than cylinders/tubes. After a time a relatively sudden second process occurs in which a network of thicker fibres forms, which are observable by optical (dark field) microscopy, as well as cryo-TEM and SAXS.

The molecular arrangement within gelator fibres is a perennial point of discussion and for the most part analogy to known single crystal X-ray structures, either of the gelator itself or structural analogues is made. Indeed, the expected packing of molecules within the fibres is of stacks where all three amides form intermolecular hydrogen bonds as observed in the crystal structure reported for **CH-Tyr**. Experimental evidence in support of such a model for the arrangements of monomer in the gel fibres comes from the diffraction pattern obtained by cryo-TEM and the similarity in the polarization dependence of the Raman spectra of the fibres and crystals of **CH-Tyr**.

The formation of fibres occurs only above the CGC. Below this concentration precipitation and/or crystallization prevails, consistent with fibre formation favoured kinetically and the crystallization the thermodynamic product. The fibres when formed continue to grow in thickness by laterally in addition to rapid longitudinal extension, as apparent from cryo-TEM micrographs where ribbons are seen with uniform intensity over the breadth and the improved fit of SAXS data using a tape model over a cylindrical model. This increase in breadth over time can be ascribed to Ostwald ripening at the expense of smaller fibres by dissolution and crystallization on the main fibre or, less probable, by zipping of small fibres together. This model is consistent with the broad distribution of fibre widths after 24 h (over 50 nm). Notably however, the dissolved monomers present in the formed gels (ca. 10%) do not show broadening, indicating interchange of monomer in and out of the gel fibres is slow with respect to the NMR timescale and hence dissolution and regrowth is at most slow. The cause of the preferred direction of growth (i.e. anisotropic along all three axes) may arise from the involvement of the carboxylic acid groups at the periphery of the gelator, which bind

to cations in the gel (Na^+) with the periphiral acid groups. Indeed the importance of this interaction to gel strength was highlighted earlier by us in the correlation between cation size and gel strength,[17] and the crystal structure of **CH-Tyr**, in which two K^+ ions stabilize the packing and the increase in symmetry observed in the polarized Raman spectra of the fibres.

Conclusion

The rational design of functional molecular systems requires that interactions between components are understood at several length scales, from molecular packing to inter-fibre interactions. However, the dynamic nature of self-assembled systems and especially the importance of meta-stable states means that design must consider kinetic aspects of the processes involved also. The use of molecular probes and especially luminescent compounds to follow these processes has the key drawback that they can disturb the very supramolecular interactions that are under study, i.e. they are not necessarily innocent reporters. In this study, the direct observation of self-assembly without the use of such probes (i.e. label free) using a combination of DFM to follow the gelation of **CH-Abu** and **CH-Leu** from dissolved state to fully formed gels was coupled with analysis of growth at the nanometer scale by cryo-TEM (static) and SAXS (dynamic). The combination of techniques reveal that short thin fibres form almost immediately after pH jumping and only later does an increase in length and thickness occur forming the stable gel. Molecular packing in the gel fibres was confirmed by comparison of single crystals, for which the structures have been determined, and polarized Raman microspectroscopy. The latter confirmed that the gelator molecules pack in the fibres in a similar (stacked) manner as found in crystals of **CH-Tyr** but notably do not pack in the same manner as in crystals of **CH-Abu** itself. This difference highlights the risk in drawing analogy between crystal structures and packing in supramolecular systems without additional direct evidence. The combination of techniques used gives us direct evidence for the gelation mechanism and a total overview of all the processes that can happen during the transistion from soluble and insoluble. In the present system the key observation is that precipitation precedes the growth of the stable gel fibre bundles, which is counter to expectations for a kinetically controlled process. These data indicate that the anisotropy in the strength of intermolecular interactions can overcome precipitation and that gel formation can proceed through several stages before the final stable form is obtained.

Acknowledgments

We thank the staffs from BL16B1 and BL19U2 (beamline of National Facility of Protein Science Shanghai (NFPS)) at Shanghai Synchrotron Radiation Facility, for assistance during data collection. We thank dr. Marc C.A. Stuart for his help with Cryo-TEM measurements, prof. Qian Li and prof. XiaoGuo Liu for their help with measuring SAXS data, prof. Giuseppe Portale for analyzing the SAXS data, and prof. Edwin Otten for measuring single crystal X-Ray of CH-Abu.

Bibliography

(1) Annabi, N.; Tamayol, A.; Uquillas, J. A.; Akbari, M.; Bertassoni, L. E.; Cha, C.; Camci-Unal, G.; Dokmeci, M. R.; Peppas, N. a.; Khademhosseini, A. 25th Anniversary Article: Rational Design and Applications of Hydrogels in Regenerative Medicine. *Adv. Mater.* **2014**, *26*, 85–124. https://doi.org/10.1002/adma.201303233.

(2) Murphy, N. P.; Lampe, K. J. Mimicking Biological Phenomena in Hydrogel- Based Biomaterials to Promote Dynamic Cellular Responses. *J. Mater. Chem. B* **2015**, *3*, 7867–7880. https://doi.org/10.1039/C5TB01045D.

(3) Du, X.; Zhou, J.; Shi, J.; Xu, B. Supramolecular Hydrogelators and Hydrogels: From Soft Matter to Molecular Biomaterials. *Chem. Rev.* **2015**, *115* (24), 13165–13307. https://doi.org/10.1021/acs.chemrev.5b00299.

(4) Ulbrich, K.; Holá, K.; Šubr, V.; Bakandritsos, A.; Tuček, J.; Zbořil, R. Targeted Drug Delivery with Polymers and Magnetic Nanoparticles: Covalent and Noncovalent Approaches, Release Control, and Clinical Studies. *Chem. Rev.* **2016**, *116*, 5338–5431. https://doi.org/10.1021/acs.chemrev.5b00589.

(5) Buwalda, S. J.; Boere, K. W. M.; Dijkstra, P. J.; Feijen, J.; Vermonden, T.; Hennink, W. E. Hydrogels in a Historical Perspective: From Simple Networks to Smart Materials. *J. Control. Release* **2014**, *190*, 254–273. https://doi.org/10.1016/j.jconrel.2014.03.052.

(6) Mendes, P. M. Stimuli-Responsive Surfaces for Bio-Applications. *Chem. Soc. Rev.* **2008**, *37* (11), 2512. https://doi.org/10.1039/b714635n.

(7) Stuart, M. A. C.; Huck, W. T. S.; Genzer, J.; Müller, M.; Ober, C.; Stamm, M.; Sukhorukov, G. B.; Szleifer, I.; Tsukruk, V. V.; Urban, M.; et al. Emerging Applications of Stimuli-Responsive Polymer Materials. *Nat. Mater.* **2010**, *9* (2), 101–113. https://doi.org/10.1038/nmat2614.

(8) Döring, A.; Birnbaum, W.; Kuckling, D. Responsive Hydrogels – Structurally and Dimensionally Optimized Smart Frameworks for Applications in Catalysis, Micro-System Technology and Material Science. *Chem. Soc. Rev.* **2013**, *42* (17), 7391. https://doi.org/10.1039/c3cs60031a.

(9) Koetting, M. C.; Peters, J. T.; Steichen, S. D.; Peppas, N. A. Stimulus-Responsive Hydrogels: Theory, Modern Advances, and Applications. *Mater. Sci. Eng. R Reports* **2015**, *93*, 1–49. https://doi.org/10.1016/j.mser.2015.04.001.

(10) Zhao, D.; Moore, J. S. Nucleation-Elongation: A Mechanism for Cooperative Supramolecular Polymerization. *Org. Biomol. Chem.* **2003**, *1* (20), 3471–3491. https://doi.org/10.1039/b308788c.

(11) De Greef, F.A., Smulders, M.J., Wolffs, M., Schenning, A.P..H.J., Sijbesma, R.P., Meijers, E. W.; De Greef, T. F. A.; Smulders, M. M. J.; Wolffs, M.; Schenning, A. P. H. J.; Sijbesma, R. P.; Meijer, E. W. Supramolecular Polymerization. *Chem. Rev.* **2009**, *109* (11), 5687–5754. https://doi.org/10.1021/cr900181u.

(12) Besenius, P.; Portale, G.; Bomans, P. H. H.; Janssen, H. M.; Palmans, A. R. A.; Meijer, E. W. Controlling the Growth and Shape of Chiral Supramolecular Polymers in Water. *Proc. Natl. Acad. Sci.* **2010**, *107* (42), 17888–17893. https://doi.org/10.1073/pnas.1009592107.

(13) Wang, F.; Gillissen, M. A. J.; Stals, P. J. M.; Palmans, A. R. A.; Meijer, E. W. Hydrogen Bonding Directed Supramolecular Polymerisation of Oligo(Phenylene-Ethynylene)s: Cooperative Mechanism, Core Symmetry Effect and Chiral Amplification. *Chem. - A Eur. J.* **2012**, *18* (37), 11761–11770. https://doi.org/10.1002/chem.201200883.

(14) Gillissen, M. A. J. J.; Koenigs, M. M. E. E.; Spiering, J. J. H. H.; Vekemans, J. A. J. M. J. M.; Palmans, A. R. A. A.; Voets, I. K.; Meijer, E. W. Triple Helix Formation in Amphiphilic Discotics: Demystifying Solvent Effects in Supramolecular Self-Assembly. *J. Am. Chem. Soc.* **2014**, *136* (1), 336–343. https://doi.org/10.1021/ja4104183.

(15) Draper, E. R.; Morris, K. L.; Little, M. A.; Raeburn, J.; Colquhoun, C.; Cross, E. R.; McDonald, T. O.; Serpell, L. C.; Adams, D. J. Hydrogels Formed from Fmoc Amino Acids. *CrystEngComm* **2015**, *17* (42), 8047–8057. https://doi.org/10.1039/C5CE00801H.

(16) Kulkarni, C.; Meijer, E. W.; Palmans, A. R. A. Cooperativity Scale: A Structure–Mechanism Correlation in the Self-Assembly of Benzene-1,3,5-Tricarboxamides. *Acc. Chem. Res.* **2017**, *50* (8), 1928–1936. https://doi.org/10.1021/acs.accounts.7b00176.

(17) Canrinus, T. R.; Cerpentier, F. J. R.; Feringa, B. L.; Browne, W. R. Remarkable Solvent Isotope Dependence on Gelation Strength in Low Molecular Weight Hydro-Gelators. *Chem. Commun.* **2017**, *53* (10), 1719–1722. https://doi.org/10.1039/C7CC00017K.

(18) Lightfoot, M. P.; Mair, F. S.; Pritchard, R. G.; Warren, J. E. New Supramolecular Packing Motifs : π-Stacked Rods Encased in Triply-Helical Hydrogen Bonded Amide Strands Using a Novel Conjunction of Organizational Motifs into a p - Bonds , in a Manner Suggestive of a New Mode of Organization. *Chem. Commun.* **1999**, 1945–1946.

(19) van Bommel, K. J. C.; van der Pol, C.; Muizebelt, I.; Friggeri, A.; Heeres, A.; Meetsma, A.; Feringa, B. L.; van Esch, J. Responsive Cyclohexane-Based Low-Molecular-Weight Hydrogelators with Modular Architecture. *Angew. Chem. Int. Ed.* **2004**, *43* (13), 1663–1667. https://doi.org/10.1002/anie.200352396.

(20) Draper, E. R.; Adams, D. J. Low-Molecular-Weight Gels: The State of the Art. *Chem* **2017**, *3* (3), 390–410. https://doi.org/10.1016/j.chempr.2017.07.012.

(21) Raeburn, J.; Mendoza-Cuenca, C.; Cattoz, B. N.; Little, M. A.; Terry, A. E.; Zamith Cardoso, A.; Griffiths, P. C.; Adams, D. J. The Effect of Solvent Choice on the Gelation and Final Hydrogel Properties of

Fmoc–Diphenylalanine. *Soft Matter* **2015**, *11* (5), 927–935. https://doi.org/10.1039/C4SM02256D.

(22) van Bommel, K. J. C.; van Esch, J. H.; De Loos, M.; Heeres, A.; Feringa, B. L. Gelling Agents. WO 03/097587 A2, 2002.

(23) Heeres, A.; van der Pol, C.; Stuart, M.; Friggeri, A.; Feringa, B. L.; van Esch, J. Orthogonal Self-Assembly of Low Molecular Weight Hydrogelators and Surfactants. *J. Am. Chem. Soc.* **2003**, *125* (47), 14252–14253. https://doi.org/10.1021/ja036954h.

(24) Friggeri, A.; van der Pol, C.; van Bommel, K. J. C.; Heeres, A.; Stuart, M. C. A.; Feringa, B. L.; van Esch, J. Cyclohexane-Based Low Molecular Weight Hydrogelators: A Chirality Investigation. *Chem. - A Eur. J.* **2005**, *11* (18), 5353–5361. https://doi.org/10.1002/chem.200500007.

(25) De Jong, M.; Winckels, J. H. F. Controlled Release Gels. EP 1800694A1, 2007.

(26) Brizard, A.; Stuart, M.; Van Bommel, K.; Friggeri, A.; De Jong, M.; Van Esch, J. Preparation of Nanostructures by Orthogonal Self-Assembly of Hydrogelators and Surfactants. *Angew. Chem. Int. Ed.* **2008**, *47* (11), 2063–2066. https://doi.org/10.1002/anie.200704609.

(27) Boekhoven, J.; Poolman, J. M.; Maity, C.; Li, F.; van der Mee, L.; Minkenberg, C. B.; Mendes, E.; van Esch, J. H.; Eelkema, R. Catalytic Control over Supramolecular Gel Formation. *Nat. Chem.* **2013**, *5* (5), 433–437. https://doi.org/10.1038/nchem.1617.

(28) Lovrak, M.; Hendriksen, W. E. J.; Maity, C.; Mytnyk, S.; Van Steijn, V.; Eelkema, R.; Van Esch, J. H. Free-Standing Supramolecular Hydrogel Objects by Reaction-Diffusion. *Nat. Commun.* **2017**, *8*, 1–9. https://doi.org/10.1038/ncomms15317.

(29) Noteborn, W. E. M.; Zwagerman, D. N. H.; Talens, V. S.; Maity, C.; van der Mee, L.; Poolman, J. M.; Mytnyk, S.; van Esch, J. H.; Kros, A.; Eelkema, R.; et al. Crosslinker-Induced Effects on the Gelation Pathway of a Low Molecular Weight Hydrogel. *Adv. Mater.* **2017**, *29* (12), 1603769. https://doi.org/10.1002/adma.201603769.

(30) Dubochet, J.; Adrian, M.; Chang, J.-J.; Lepault, J.; McDowall, A. W. Cryoelectron Microscopy of Vitrified Specimens. In *Cryotechniques in Biological Electron Microscopy*; Springer Berlin Heidelberg: Berlin, Heidelberg, 1987; Vol. 2, pp 114–131. https://doi.org/10.1007/978-3-642-72815-0_5.

(31) Glatter, O.; Kratky, O. *Small Angle X-Ray Scattering*; 1982.

(32) Martens, A. A.; Portale, G.; Werten, M. W. T.; De Vries, R. J.; Eggink, G.; Cohen Stuart, M. A.; De Wolf, F. A. Triblock Protein Copolymers Forming Supramolecular Nanotapes and PH-Responsive Gels. *Macromolecules* **2009**, *42* (4), 1002–1009. https://doi.org/10.1021/ma801955q.

(33) Fan, E.; Yang, J.; Geib, S. J.; Stoner, T. C.; Hopkins, M. D.; Hamilton, A. D. Hydrogen-Bonding Control of Molecular Aggregation: Self-Complementary Subunits Lead to Rod-Shaped Structures in the Solid State. *J. Chem. Soc. Chem. Commun.* **1995**, *4* (12), 1251. https://doi.org/10.1039/c39950001251.

4